APL Photonics

RESEARCH ARTICLE | OCTOBER 16 2024

Mid-infrared hyperspectral microscopy with broadband 1-GHz dual frequency combs

Special Collection: Mid-IR Photonics

Peter Chang ; Ragib Ishrak ; Nazanin Hoghooghi ; Scott Egbert ; Daniel Lesko ; Stephanie Swartz ; Jens Biegert ; Gregory B. Rieker ; Rohith Reddy; Scott A. Diddams

APL Photonics 9, 106111 (2024)
https://doi.org/10.1063/5.0225616

Mid-infrared hyperspectral microscopy with broadband 1-GHz dual frequency combs

Cite as: APL Photon. 9, 106111 (2024); doi: 10.1063/5.0225616
Submitted: 25 June 2024 • Accepted: 15 September 2024 •
Published Online: 16 October 2024

Peter Chang,[1,2,a)] Ragib Ishrak,[3] Nazanin Hoghooghi,[4,5] Scott Egbert,[4] Daniel Lesko,[6] Stephanie Swartz,[5] Jens Biegert,[7,8] Gregory B. Rieker,[4] Rohith Reddy,[3] and Scott A. Diddams[1,2,b)]

AFFILIATIONS

[1] Department of Electrical, Computer and Energy Engineering, University of Colorado at Boulder, Boulder, Colorado 80309, USA
[2] Department of Physics, University of Colorado at Boulder, Boulder, Colorado 80309, USA
[3] Department of Electrical and Computer Engineering, University of Houston, Houston, Texas 77204, USA
[4] Department of Mechanical Engineering, University of Colorado at Boulder, Boulder, Colorado 80309, USA
[5] Time and Frequency Division, National Institute of Standards and Technology, Boulder, Colorado 80305, USA
[6] Department of Chemistry, University of Colorado at Boulder, Boulder, Colorado 80309, USA
[7] ICFO - Institut de Ciencies Fotoniques, The Barcelona Institute of Science and Technology, Castelldefels 08860, Barcelona, Spain
[8] ICREA, Pg. Lluís Companys 23, 08010 Barcelona, Spain

Note: This paper is part of the APL Photonics Special Topic on Mid-IR Photonics.
[a)] **Author to whom correspondence should be addressed:** peter.chang-1@colorado.edu
[b)] **E-mail:** scott.diddams@colorado.edu

ABSTRACT

Mid-infrared microscopy is an important tool for biological analyses, allowing a direct probe of molecular bonds in their low energy landscape. In addition to the label-free extraction of spectroscopic information, the application of broadband sources can provide a third dimension of chemical specificity. However, to enable widespread deployment, mid-infrared microscopy platforms need to be compact and robust while offering high speed, broad bandwidth, and high signal-to-noise ratio. In this study, we experimentally showcase the integration of a broadband, high-repetition-rate dual-comb spectrometer (DCS) in the mid-infrared range with a scanning microscope. We employ a set of 1-GHz mid-infrared frequency combs, demonstrating their capability for high-speed and broadband hyperspectral imaging of polymers and ovarian tissue. The system covers 1000 cm^{-1} at ν_c = 2941 cm^{-1} with 12.86 kHz spectra acquisition rate and 5 μm spatial resolution. Taken together, our experiments and analysis elucidate the trade-off between bandwidth and speed in DCS as it relates to microscopy. This provides a roadmap for the future advancement and application of high-repetition-rate DCS hyperspectral imaging.

I. INTRODUCTION

Vibrational spectroscopy is a cornerstone technique for molecular characterization that provides detailed insights into molecular structures, interactions, and dynamics. Essentially, it identifies the unique vibrational "fingerprints" of molecules, revealing their specific characteristics and behaviors. While this method provides deep insights into the molecular makeup, spectroscopic imaging has enhanced its scope. Spectroscopic imaging marries the depth of vibrational spectroscopy with a spatial context, presenting a combined image where one can pinpoint not just which molecules are present but also their exact locations. This enhanced perspective is invaluable across diverse fields, from understanding material properties to probing biological systems, facilitating a richer and more precise understanding of intricate molecular landscapes.

Within this context, vibrational spectroscopy using mid-infrared light (~3–12 μm) proves beneficial in bio-imaging because it provides label-free chemical contrast and can non-invasively identify the biomolecular composition of samples.[1] Tissues, cells, and other biological entities can be analyzed without external dyes

or markers, preserving the sample's native state. This is essential in clinical applications, where assessing the safety and efficacy of external contrast agents can be challenging. Spectroscopic imaging can complement conventional diagnostic techniques as the sample remains undisturbed. While spectroscopic imaging offers invaluable chemical insights, its slow signal acquisition has hindered its widespread adoption in biomedical and clinical settings.[2–4] The trade-off between speed and bandwidth in recent systems based on mid-infrared laser sources can compromise its competitiveness against label-based fluorescence microscopy, the principal bio-imaging technology.

In this work, we introduce and explore the capabilities of dual comb spectroscopy (DCS)[5] for mid-infrared hyperspectral microscopy. Our work utilizes a set of recently developed 1 GHz mid-infrared frequency combs[6] to integrate a dual-comb spectrometer with a confocal microscope. We capitalize on the 1 GHz repetition rate of the combs for rapid data acquisition to capture a full spectrum across 2595–3890 cm^{-1} every 78 μs (corresponding to a dual-comb repetition rate difference of Δf_r = 12.86 kHz). As such, the system is among the fastest performers in the class of spectrometers covering over 1000 cm^{-1} in the mid-infrared, while maintaining 1 GHz (0.03 cm^{-1}) spectral resolution.

II. LANDSCAPE OF MID-INFRARED HYPERSPECTRAL IMAGING

The effort to push the barrier of spectral acquisition speed without compromising bandwidth is illustrated in Fig. 1, which provides a visual overview of significant developments in hyperspectral vibrational imaging over the past two decades. Experiments are mapped onto the two important metrics of spectra: acquisition speed, which captures the rate at which a single spectrum is gathered, and optical bandwidth, which captures the breadth of chemical content that can be observed. The two variables are plotted against each other since a significant difficulty lies in achieving both metrics simultaneously. For a better one-to-one comparison, the experiments that use focal plane arrays have been adjusted to show the time required to acquire a single spectrum at one point.

The scope of Fig. 1 is restricted to experiments that have already demonstrated hyperspectral microscopy in the mid-infrared. This reduction from the full breadth of imaging and spectroscopy modalities is important, due to the challenges of developing and realizing both spectroscopy and microscopic imaging in a single platform. For instance, absent from the diagram is time-stretch spectroscopy, which has achieved a maximum spectral acquisition rate equal to the repetition rate of the laser (e.g., hundreds of MHz to multiple GHz).[7] However, hyperspectral imaging with this technique has not yet been implemented in the mid-infrared, in part because of the lack of good detectors as well as the challenge of producing well-controlled group-velocity dispersion over bandwidths approaching 1000 cm^{-1} (Ref. 8). We note that the utilization of upconversion to the near-infrared[9,10] or coherent Stokes Raman scattering[11] can extend the applicability of time-stretch spectroscopy to longer wavelengths. Another technique is the advanced rapid scan type of FT-IR[12] and FT-CARS,[13] which can significantly increase the mechanical scan

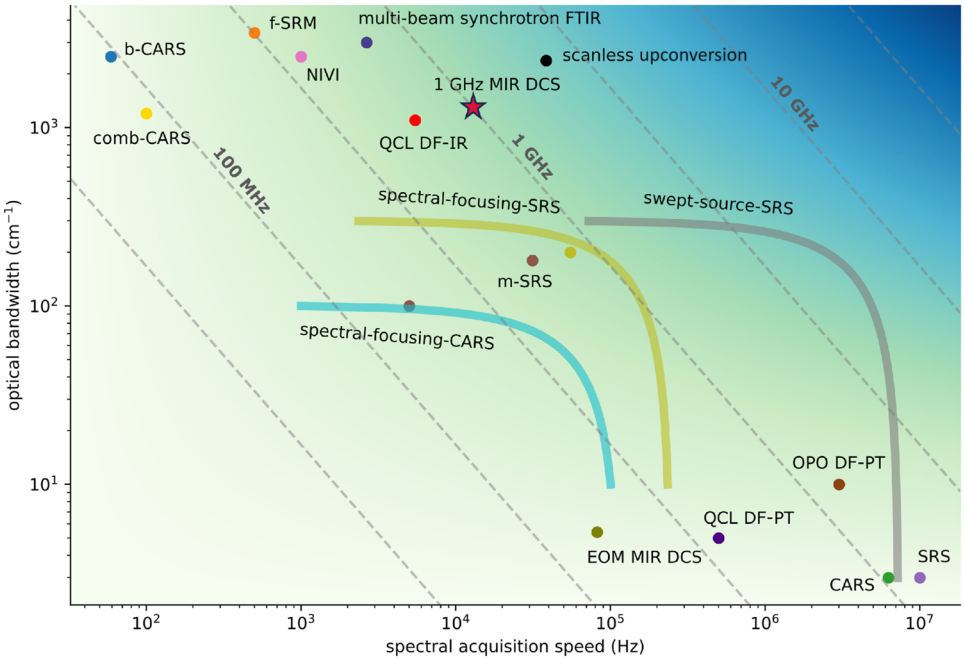

FIG. 1. Performance map of mid-infrared hyperspectral imaging. As a guideline relevant to this work, the diagonal dashed lines show the $f_r^2/2$ trade-off inherent to DCS. Broadband CARS (b-CARS),[14] femtosecond Stimulated Raman Microscopy (f-SRM),[15] *in vivo* video rate CARS,[16] *in vivo* video rate SRS,[17] multiplexed SRS (*m*-SRS),[18,19] nonlinear interferometric vibrational imaging (NIVI),[20] swept-source SRS,[21] spectral-focusing SRS,[22,23] spectral-focusing CARS,[24] comb-CARS,[25] multi-beam synchrotron FTIR,[26] electro-optic modulator comb MIR DCS,[27] QCL discrete frequency infrared imaging (DF-IR),[4] QCL discrete frequency photothermal imaging (QCL DF-PT),[28] OPO discrete frequency photothermal imaging (OPO DF-PT),[29] and scanless mid-infrared upconversion imaging.[30]

rate of the classical FT-IR interferometer. However, to the best of our knowledge, these spectroscopy approaches have not yet been employed in a mid-infrared microscope.

With the focus on microscopic imaging, coherent Raman spectro-imaging has achieved *in vivo* video-rate speeds in the mid-infrared[16,17] using well-established near-infrared femtosecond oscillators. Whereas initial demonstrations were over a narrow bandwidth (~3 cm^{-1}), broad bandwidths at high acquisition speeds have been achieved using rapidly rotating polygonal mirror scanners.[23,31] The high metrics are possible with the strong Raman absorption cross sections around 2900 cm^{-1}. It is challenging, however, for Raman spectroscopy-based platforms to reach the same performance in the fingerprint region at longer wavelengths. An important target, therefore, is to achieve a similar performance with direct mid-infrared illumination.

Fourier transform spectroscopy (FTS) and quantum cascade laser (QCL) based imaging are attractive due to their broad applicability across the mid- to long wavelength infrared. The high absorption cross sections alleviate the need for operation at powers close to sample-damage thresholds, a concern that is applicable to biological samples. In this category, FTS spectrometers coupled to broadband and bright sources such as synchrotron facilities have set the state-of-the-art for the combination of spectral bandwidth and speed.[26] However, a widely accessible imaging method would benefit from having a table top setup. To address this, QCLs are attractive due to their direct emission in the mid-infrared and small footprint, although their performance is best leveraged in narrowband applications. Recent experiments demonstrating photothermal imaging with single wavelength QCLs have achieved video rate speeds at sub-diffraction limit spatial resolution.[28] Tunable QCL packages consisting of multiple QCL chips combined into one device[4,32,33] can reach broad spectral coverage, but a further improvement is needed to reach noise figures comparable to platforms based on mode-locked lasers.

An alternative method to boost imaging speed in the mid-infrared is to employ upconversion to shorter wavelengths in order to leverage low-cost near-infrared cameras, whose performance can significantly exceed mid-infrared focal plane arrays.[34–36] A recent demonstration covered > 1000 cm^{-1} in 8 s.[30] However, a potential drawback to this platform is a demand for very high pump pulse energies on the millijoule scale, requiring large regenerative amplifiers and a bulky apparatus.

Alongside scanless methods, the concept of a compact and deployable imaging system motivates parallel development of platforms seeded by well-developed fiber-integrated light sources. Fiber oscillators and amplifiers in the near infrared (for example, in the 1550 nm telecommunication band) are compact, robust, and alignment free. However, their pulse energies typically fall in the 1–10 nJ range. This necessitates well-designed nonlinear optics to translate to the mid-infrared, as well as the development of techniques separate from existing scanless imaging.

In this work, we explore and apply high rep-rate dual-comb spectroscopy (DCS) to hyperspectral imaging. DCS has emerged as a powerful technique due to its combination of resolution, stability, and speed when compared to classical FTS.[5] In this modality, the interference of two frequency combs maps a Nyquist band from the optical domain down into the RF. One of the most important considerations in DCS is the direct trade-off between the repetition rate f_r and the size of the optical Nyquist window created by the interference of the comb lines $\Delta\nu$,

$$\Delta\nu = \frac{f_r^2}{2\Delta f_r}, \tag{1}$$

where Δf_r is the interferogram acquisition rate equal to the difference of the two laser rep-rates. The diagonal dashed lines in Fig. 1 show the $f_r^2/2$ trade-off between resolvable bandwidth and acquisition speed in DCS for different f_r. Evidently, when the broad absorption features of large condensed phase molecules such as lipids and proteins allow for coarse resolution, the highest rep-rates exceeding 1 GHz are desired.

As highlighted by the void in the upper right region of Fig. 1, hyperspectral imaging that simultaneously affords 1000 cm^{-1} coverage at megahertz acquisition rates is challenging to achieve. However, this presents an opportunity for scanned imaging with DCS platforms, provided the existence of broad bandwidth mid-infrared frequency combs with 10 GHz mode spacing. Generally speaking, this is a challenging regime for frequency combs, although such mode-spacings can be realized on electro-optic modulator (EOM) platforms[37] and in a few cases have even been used for imaging.[27,38] EOM combs spanning bandwidths greater than 1000 cm^{-1} at 10 GHz have been demonstrated in the near-infrared,[39] but a challenge remains in efficient and broad bandwidth downconversion to the mid-infrared.[37] On an integrated platform, microcombs[40,41] can generate coherent frequency combs spanning up to a few hundred wavenumber. However, coverage well past $\lambda \approx 3$ μm (3333 cm^{-1}) remains an outstanding challenge for microcombs. Nonetheless, this is a promising direction to explore, and our present effort with 1 GHz mid-infrared dual comb imaging is a step toward even higher bandwidths and acquisition rates as given by Eq. (1).

III. ROADMAP FOR IMAGING SPEED WITH DCS

Whereas Fig. 1 illustrates the significant challenge of optical bandwidth and spectral acquisition rate, it does not fully capture the metric of imaging speed, which in the end is determined by the averaging time needed to reach sufficient signal-to-noise ratio (SNR) at each pixel. Consequently, it is useful to have an experimentally driven map of imaging speed in the relevant case of point scanning dual-comb microscopy, where the target SNR and frequency resolution sets the pixel dwell time.

In DCS, the absorbance noise σ scales with the frequency resolution and number of averaged spectra N_{avg} according to Ref. 42,

$$\sigma \propto \frac{N}{\sqrt{N_{avg}}}\sqrt{\epsilon}, \tag{2}$$

where N is the number of frequency bins and $\epsilon = \nu_{res}/f_r$ is referred to as the duty cycle, where ν_{res} is the frequency resolution and f_r is the repetition rate. We note that $\epsilon \geq 1$ and only approaches unity for the case of mode-resolved spectroscopy with $\nu_{res} = f_r$, and otherwise increases with apodization according to $\epsilon \propto 1/N$. The scaling rule for σ is shown in Fig. 2(c), where it is observed to match the experimentally measured absorbance noise. Importantly, Eq. (2) entails a square root scaling improvement in SNR $\propto 1/\sigma$ for both the number of averaged spectra and apodization of interferograms

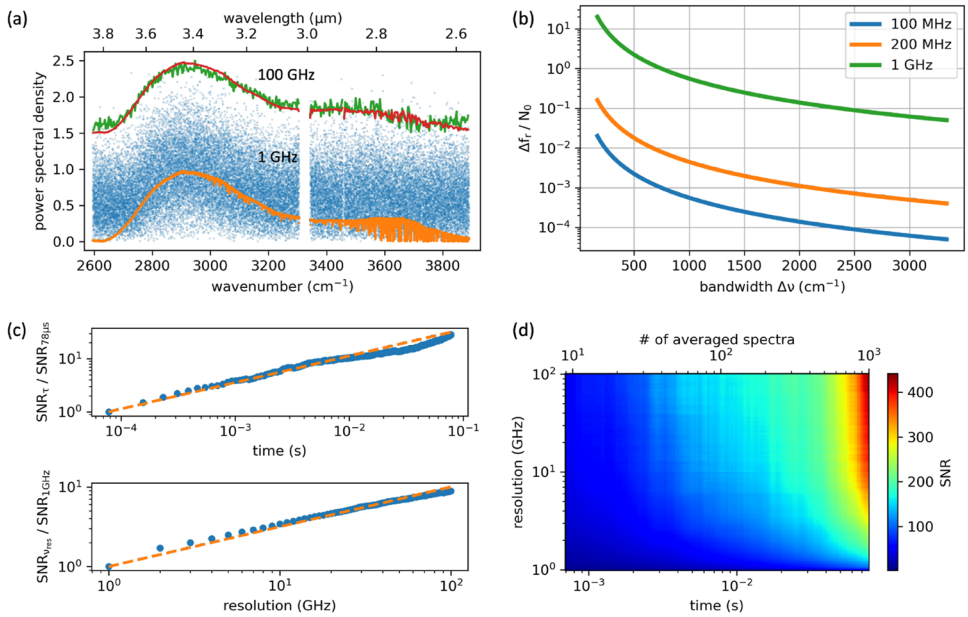

FIG. 2. Summary of DCS imaging speed. (a) DCS spectra taken at different averaging times and frequency resolution/apodization windows. A single-shot spectrum at 1 GHz resolution (blue/green) can be averaged to a high SNR (orange/red) in 2 s, or in 39 ms at 100 GHz resolution. The lines in the higher resolution spectrum are due to water absorption. (b) The spectra acquisition rate divided by the fundamental number of frequency bins, $N_0 = \Delta\nu/f_r$, plotted against the size of the optical Nyquist window. Three curves are shown for different repetition rates. (c) The relative SNR improvement from signal averaging and apodization. The orange dashed curves mark the theoretical square root scaling. (d) The 2D SNR parameter space of signal averaging and apodization [combining the two plots in (c)] for the 1-GHz system.

(decreasing N). The artificial resolution is penalized by the factor of $\sqrt{\epsilon}$, which softens the benefit of apodization to an effective $1/\sqrt{N}$ scaling. A directly proportional scaling improvement can be achieved, however, if one moves to a higher rep-rate source with larger mode-spacing.

This is illustrated in Fig. 2(a) for the case of 1 GHz frequency combs. A baseline for 1 GHz DCS is that a 1000 cm^{-1} Nyquist window can be covered with ~17 kHz spectra acquisition speed. In Fig. 2(a), a single-shot spectrum (78 μs) at 1 GHz resolution has low signal to noise but can be averaged to a high SNR in 2 s (>25 000 spectra). However, SNR > 200 can also be achieved in ~39 ms at 500 averages if the interferograms are apodized to 100 GHz (~3.33 cm^{-1}), which is a more appropriate sampling interval for condensed phase and bio-relevant absorption features. The SNR as a function of averaging time and apodized frequency resolution is shown in Figs. 2(c) and 2(d). The absorbance noise averages down according to $1/\sqrt{N_{avg}}$ and with coarser resolution, resulting in a similar $1/\sqrt{N}$ noise reduction.

More importantly, this experimental analysis of bandwidth, SNR, frequency resolution, and imaging speed provides a roadmap for the integration of high rep-rate sources into the field of microscopy (Fig. 1). The time, τ_{ifg}, to acquire a single spectrum or interferogram decreases with the rep-rate according to $\tau_{ifg} \propto 1/f_r^2$. However, an important additional consideration is the direct $\sigma \propto N$ improvement gained from the coarser resolution, compared to the $\sigma \propto \sqrt{N}$ improvement in the case of apodization. Practically speaking, for an equivalent optical Nyquist band, the consideration of SNR adds an additional f_r scaling to the well-known $\Delta f_r \propto f_r^2$ [Eq. (1)], leading to an overall, and very favorable, f_r^3 scaling with the mode-spacing [Fig. 2(b)]. As an example, in our previous work with 100 MHz mid-infrared DCS,[43,44] a comparable SNR was reached with ~ 1 min averaging per pixel, whereas a potential 10 GHz DCS platform can reach the same SNR in 39 μs, reducing the overall experiment time from several hours in this experiment down to ~10 s.

IV. EXPERIMENT AND RESULTS

With simplicity and long-term stability in mind, a single-branch intra-pulse difference frequency generation (IP-DFG) design is used to generate frequency comb light in the mid-infrared.[6,37,43] The architecture of a single mid-infrared comb source is illustrated in the upper part of Fig. 3. The 1 GHz mode-locked laser is amplified to 4 W and launched into a highly nonlinear fiber (HNLF). Soliton self-compression in the anomalous dispersion HNLF results in octave-spanning, few cycle near-infrared (NIR) pulses that efficiently drive the nonlinear intra-pulse downconversion to the mid-infrared. The offset frequency and repetition rate of the frequency comb are controlled via servo loops. Further details are given in earlier publications.[6,45] Ideally, full use of the laser bandwidth would entail coverage of the molecular fingerprint region as shown previously for one laser system[6] and also studied at lower rep-rates with IP-DFG.[46,47] However, in this work, more widely available lithium niobate is used to reach the 3–5 μm wavelength window, which covers the C–H stretch region at ~2920 cm^{-1}.

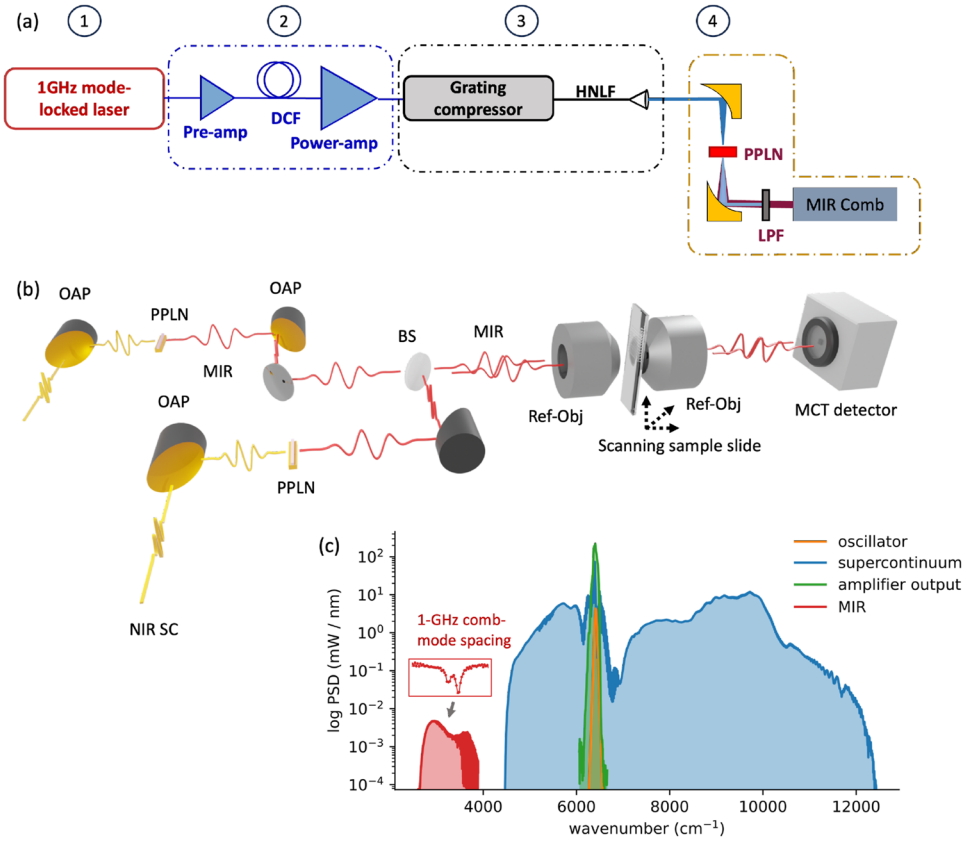

FIG. 3. Experimental setup. (a) Approach to generate mid-infrared frequency combs via soliton self-compression in a highly nonlinear fiber (HNLF) followed by intra-pulse difference frequency generation. (b) Two mid-infrared frequency combs generated through intra-pulse difference frequency generation in periodically poled lithium niobate (PPLN) are passed collinearly through a confocal microscope. Hyperspectral images are collected by raster scanning the sample slide. The transmitted signal is collected and digitized in a high-speed MCT mid-infrared detector and FPGA. (c) Summary of near- and mid-infrared spectral envelopes. The inset shows an example of spectroscopy of water vapor in ambient air with 1 GHz comb mode resolution.

Two 1-GHz mid-infrared frequency combs are generated in this manner and coupled into the InF_3 single-mode fiber for delivery to the experiment. The output beam is collimated with a 2 in. off-axis parabolic mirror, and a reflective confocal microscope with 0.58 NA is used to image the beam (0.7 mW) onto a glass slide (~3.8 μm pixel size). A set of linear translation stages are used to raster scan the sample. The data are acquired via trigger, with the trigger spacing and scan speed set by the desired spatial sampling interval. The scan speed is limited by the interferogram acquisition time, which is fundamentally set by the repetition rate difference of the two combs, which is servo-controlled to be 12.86 kHz. The pixel acquisition speed is limited by the rep-rate of the laser during each continuous line scan. However, there is an added few second delay for the stage to reset between each line scan, leading to faster imaging times for rectangular images. The images in Fig. 5(a) (254 × 462 pixels) and Fig. 5(c) (309 × 342 pixels) each take about one and a half hours to acquire. The transmitted signal is focused onto a high-speed MCT detector (VIGO UHSM-I-10.6) with >900 MHz electrical bandwidth, whose AC coupled port is digitized with 16 bit resolution at 1 GS/s using an FPGA (GaGe RazorMax16). The data are streamed concurrently from the card memory into PC RAM for real-time analysis such that the card-memory does not limit the data volume. Owing to the fairly high 500 MHz Nyquist frequency, and the placement of all fiber amplifiers within the physical path of the servo control loops of the two frequency combs, over one thousand interferograms can be directly averaged before phase correction needs to be employed.[48,49]

To verify the spatial resolution, hyperspectral images are taken of a USAF resolution target composed of SU-8 photoresist patterned onto a 500 μm thick silicon wafer. Five hundred spectra (acquired in 39 ms) are averaged at each pixel and apodized to 100 GHz (3.3 cm^{-1}). The point spectra shown in Fig. 4(b) are taken at each pixel to generate the hypercube. The images are generated by integrating a ~63 cm^{-1} window around the peak absorption at ~2930 cm^{-1}. Since the imaging beam is directly collimated out of single-mode fiber, a Gaussian beam treatment can be used as a good estimation of the focused beam size. The horizontal and vertical line scans across two bars in Fig. 4(c) are used as knife edge measurements[50] to determine the beam waist, giving an average of 4.45 ± 0.32 μm. This is larger than the calculated beam size of 3.8 μm, which can be

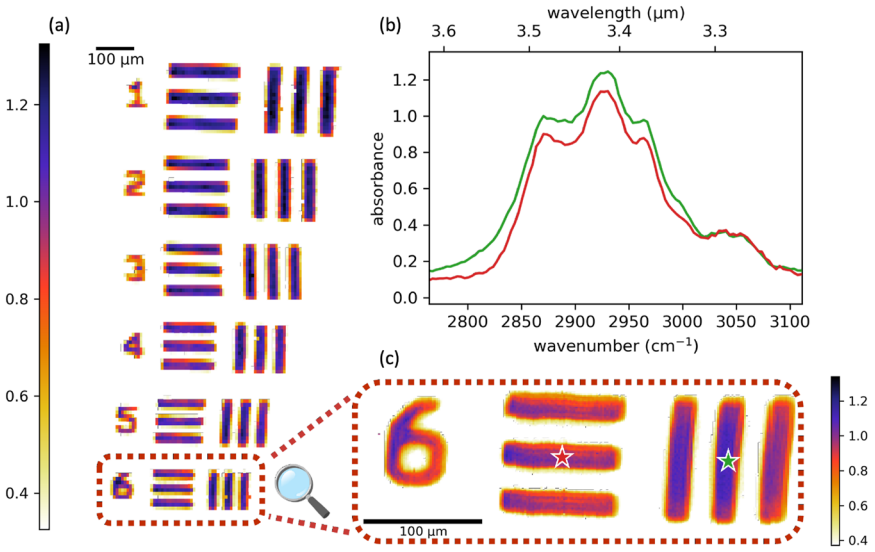

FIG. 4. Dual-comb hyperspectral image of the SU-8 USAF test pattern on silicon. (a) False-color image generated from the integrated absorbance around 2930 cm^{-1} taken at 5 μm spatial sampling. (b) Absorbance curves taken at the red and green points (stars) of panel (c), which is a magnified image taken at 1.2 μm spatial sampling.

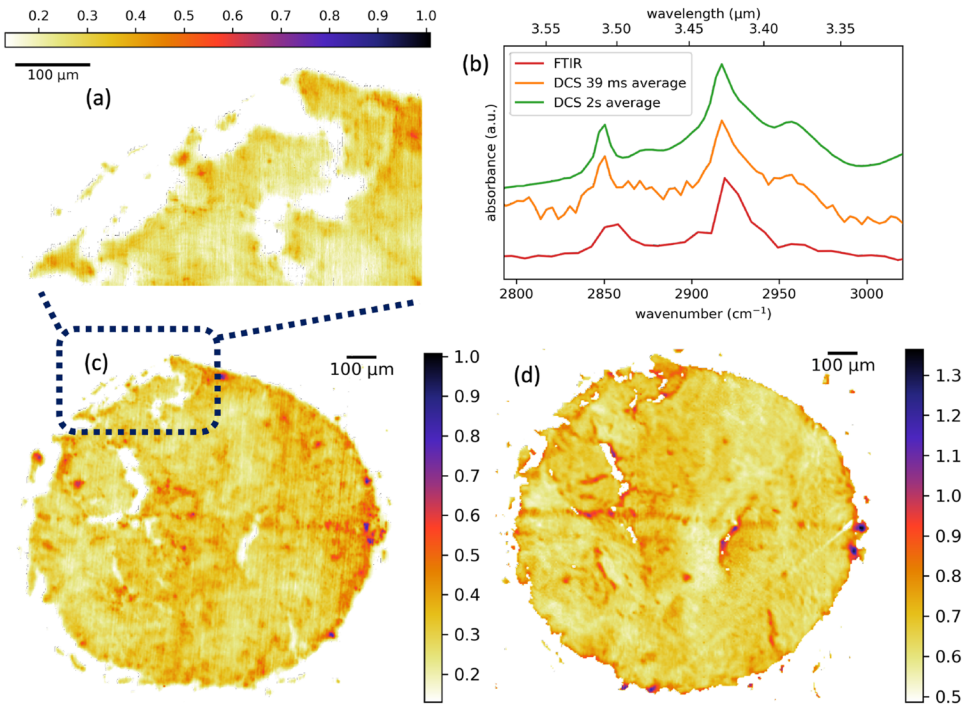

FIG. 5. Hyperspectral image of ovarian cancer tissue. (a) Absorbance at 2920 cm^{-1} taken at 1.2 μm sampling. (b) Absorbance curves taken on cancer tissue with 2 s average in green, 39 ms average in orange, and with a commercial FTIR in red. Absorbance curves have been offset for clarity. (c) Zoom out of panel (a) to include the absorbance image of the whole 1 mm core at 2920 cm^{-1} taken with 5 μm spatial sampling. (d) Equivalent image to (c) but taken using a commercial FTIR microscope with a focal plane array.

attributed to the rounded edges of the SU-8 bars, as observed in a visible microscope.

To illustrate the potential of our technique for biologically relevant samples, we image a cross section of ovarian cancer tissue. Here, we also validate our DCS point scanning hyperspectral microscopy by comparison with data taken with a commercial FTIR microscope using a focal plane array. For the DCS microscopy, 500 spectra are again averaged at each pixel and apodized to 3.3 cm^{-1}. Point spectra such as the one shown by the orange curve in Fig. 5(b) are collected at each pixel, with the two C–H anti-symmetric stretch bands visible at 2850 and 2920 cm^{-1}. A DCS spectrum taken with a 2 s averaging time (25 700 averages) is shown by the green curve, and a comparison spectrum taken using a commercial FTIR with 7.61 cm^{-1} frequency resolution is shown by the red curve. Apart from a broadening of the peak, good agreement is observed between the DCS and FTIR spectra. The FTIR image was taken prior to the removal of paraffin wax commonly used to protect tissue samples, which accounts for the image differences and peak broadening when compared to the spectra taken using DCS where no paraffin was present.

The images are generated by averaging a 10 cm^{-1} slice through the hypercube at the peak of the 2920 cm^{-1} band. A coarse image shown in Fig. 5(c) with 5 μm sampling is taken of the entire 1 mm core. A zoom-in of the sample is shown in Fig. 5(a), taken at 1.2 μm sampling. Considering the mechanical scan rate, the dwell time at each 1.2 μm pixel is ~40 ms, which is approximately the Nyquist sampling limit of the microscope. The image shows generally good agreement with the corresponding image in Fig. 5(d) taken using the FTIR microscope. We note that the dim vertical line scans in the DCS image are attributed to the limited ~1.5 μm repeatability of the translation stages (Thorlabs Z825B).

V. DISCUSSION AND CONCLUSION

In this paper, we demonstrate a high rep-rate and broadband DCS microscope covering over 1000 cm^{-1} in the 3–5 μm region of the mid-infrared. The results are used to create a performance map for future DCS applications in microscopy. In particular, we showcase the need for ultra-broadband mid-infrared frequency combs with yet higher rep-rates exceeding >10 GHz. The anticipated challenge for these sources will either be the need for significant amplification, or new nanophotonic designs whose transparency and dispersion can produce and guide light out to wavelengths covering 3–5 μm, and ideally beyond into the fingerprint region.

At a 1 GHz rep-rate, DCS brings the point scanning system's overall experiment time to comparable numbers as FTIR microscopes that employ focal plane arrays to increase their speed. In such a case, acquisition times of a few hours are needed for a 512 × 512 image after averaging at each pixel. The DCS point scanning system offers a frequency axis calibrated to an uncertainty of the measured rep-rate around 10^{-11}, whose resolution can be chosen down to the comb mode-spacing. The DCS point scanning system also offers the potential for future advances, such as multi-dimension compressed sensing. Importantly, compression could be performed not only on spatial sampling, but also spectrally by employing a time-programmable frequency comb to implement a real-time apodization, as recently shown in other systems.[8,51–53] From known work, compressively sampling the time domain interferogram could effectively push the system past the 10 GHz mode-spacing regime using digital locking electronics alone and introduce accelerated imaging times reduced by factors over a 100. We anticipate that further work in combining advanced combinations of platforms utilized by the DCS gas-sensing and imaging communities can realize a compact and robust solution to broad-band and high speed vibrational imaging.

ACKNOWLEDGMENTS

The authors acknowledge Reza Reihanisaransari for valuable help with the FTIR imaging of the ovarian cancer tissue samples. This work was supported by National Science Foundation Grant Nos. 2019195 and 2016244, AFOSR Grant No. FA9550-20-1-0328, CPRIT Grant No. RR170075, and NIH Grant Nos. R01DK135870 and R01HL173597.

AUTHOR DECLARATIONS

Conflict of Interest

The authors have no conflicts to disclose.

Author Contributions

Peter Chang: Investigation (lead); Writing – original draft (lead). **Ragib Ishrak**: Investigation (supporting); Writing – original draft (supporting). **Nazanin Hoghooghi**: Investigation (supporting); Writing – original draft (supporting). **Scott Egbert**: Investigation (supporting). **Daniel Lesko**: Investigation (supporting). **Stephanie Swartz**: Investigation (supporting). **Jens Biegert**: Conceptualization (supporting). **Gregory B. Rieker**: Conceptualization (supporting). **Rohith Reddy**: Conceptualization (supporting). **Scott A. Diddams**: Conceptualization (lead).

DATA AVAILABILITY

The data that support the findings of this study are available from the corresponding author upon reasonable request.

REFERENCES

[1]M. J. Baker, J. Trevisan, P. Bassan, R. Bhargava, H. J. Butler, K. M. Dorling, P. R. Fielden, S. W. Fogarty, N. J. Fullwood, K. A. Heys, C. Hughes, P. Lasch, P. L. Martin-Hirsch, B. Obinaju, G. D. Sockalingum, J. Sulé-Suso, R. J. Strong, M. J. Walsh, B. R. Wood, P. Gardner, and F. L. Martin, "Using Fourier transform IR spectroscopy to analyze biological materials," Nat. Protoc. **9**, 1771–1791 (2014).
[2]D. Zhang, C. Li, C. Zhang, M. N. Slipchenko, G. Eakins, and J.-X. Cheng, "Depth-resolved mid-infrared photothermal imaging of living cells and organisms with submicrometer spatial resolution," Sci. Adv. **2**, e1600521 (2016).
[3]M. R. Kole, R. K. Reddy, M. V. Schulmerich, M. K. Gelber, and R. Bhargava, "Discrete frequency infrared microspectroscopy and imaging with a tunable quantum cascade laser," Anal. Chem. **84**, 10366–10372 (2012).
[4]K. Yeh, S. Kenkel, J.-N. Liu, and R. Bhargava, "Fast infrared chemical imaging with a quantum cascade laser," Anal. Chem. **87**, 485–493 (2015).
[5]I. Coddington, N. Newbury, and W. Swann, "Dual-comb spectroscopy," Optica **3**, 414 (2016).
[6]N. Hoghooghi, S. Xing, P. Chang, D. Lesko, A. Lind, G. Rieker, and S. Diddams, "Broadband 1-GHz mid-infrared frequency comb," Light Sci. Appl. **11**, 264 (2022).

[7]K. Goda and B. Jalali, "Dispersive Fourier transformation for fast continuous single-shot measurements," Nat. Photon **7**, 102–112 (2013).
[8]A. Kawai, T. Kageyama, R. Horisaki, and T. Ideguchi, "Compressive dual-comb spectroscopy," Sci. Rep. **11**, 13494 (2021).
[9]Z. Wen, B. Peng, M. Yan, T. Zheng, Q. Wen, T. Liu, X. Ren, K. Huang, and H. Zeng, "Broadband up-conversion mid-infrared time-stretch spectroscopy," Laser Photonics Rev. **18**, 2300630 (2024).
[10]S. Yagi, T. Nakamura, K. Hashimoto, S. Kawano, and T. Ideguchi, "Mid-infrared optical coherence tomography with MHz axial line rate for real-time non-destructive testing," APL Photonics **9**, 051301 (2024).
[11]T. Ideguchi, T. Nakamura, and K. Hashimoto, "Broadband coherent Raman scattering spectroscopy at 50,000,000 spectra/s," Ultrafast Sci. (published online) (2024).
[12]K. Hashimoto, V. R. Badarla, and T. Ideguchi, "High-speed Fourier-transform infrared spectroscopy with phase-controlled delay line," Laser Photonics Rev. **15**, 2000374 (2021).
[13]K. Hashimoto, J. Omachi, and T. Ideguchi, "Ultra-broadband rapid-scan Fourier-transform CARS spectroscopy with sub-10-fs optical pulses," Opt. Express **26**, 14307 (2018).
[14]T. W. Kee and M. T. Cicerone, "Simple approach to one-laser, broadband coherent anti-Stokes Raman scattering microscopy," Opt. Lett. **29**, 2701 (2004).
[15]E. Ploetz, S. Laimgruber, S. Berner, W. Zinth, and P. Gilch, "Femtosecond stimulated Raman microscopy," Appl. Phys. B **87**, 389–393 (2007).
[16]C. L. Evans, E. O. Potma, M. Puoris'haag, D. Côté, C. P. Lin, and X. S. Xie, "Chemical imaging of tissue *in vivo* with video-rate coherent anti-Stokes Raman scattering microscopy," Proc. Natl. Acad. Sci. U.S.A. **102**, 16807–16812 (2005).
[17]B. G. Saar, C. W. Freudiger, J. Reichman, C. M. Stanley, G. R. Holtom, and X. S. Xie, "Video-rate molecular imaging in vivo with stimulated Raman scattering," Science **330**, 1368–1370 (2010).
[18]D. Fu, F.-K. Lu, X. Zhang, C. Freudiger, D. R. Pernik, G. Holtom, and X. S. Xie, "Quantitative chemical imaging with multiplex stimulated Raman scattering microscopy," J. Am. Chem. Soc. **134**, 3623–3626 (2012).
[19]C.-S. Liao, M. N. Slipchenko, P. Wang, J. Li, S.-Y. Lee, R. A. Oglesbee, and J.-X. Cheng, "Microsecond scale vibrational spectroscopic imaging by multiplex stimulated Raman scattering microscopy," Light Sci. Appl. **4**, e265 (2015).
[20]P. D. Chowdary, Z. Jiang, E. J. Chaney, W. A. Benalcazar, D. L. Marks, M. Gruebele, and S. A. Boppart, "Molecular histopathology by spectrally reconstructed nonlinear interferometric vibrational imaging," Cancer Res. **70**, 9562–9569 (2010).
[21]Y. Ozeki, W. Umemura, Y. Otsuka, S. Satoh, H. Hashimoto, K. Sumimura, N. Nishizawa, K. Fukui, and K. Itoh, "High-speed molecular spectral imaging of tissue with stimulated Raman scattering," Nat. Photon **6**, 845–851 (2012).
[22]D. Fu, G. Holtom, C. Freudiger, X. Zhang, and X. S. Xie, "Hyperspectral imaging with stimulated Raman scattering by chirped femtosecond lasers," J. Phys. Chem. B **117**, 4634–4640 (2013).
[23]H. Lin, H. J. Lee, N. Tague, J.-B. Lugagne, C. Zong, F. Deng, J. Shin, L. Tian, W. Wong, M. J. Dunlop, and J.-X. Cheng, "Microsecond fingerprint stimulated Raman spectroscopic imaging by ultrafast tuning and spatial-spectral learning," Nat. Commun. **12**, 3052 (2021).
[24]C. Di Napoli, I. Pope, F. Masia, P. Watson, W. Langbein, and P. Borri, "Hyperspectral and differential CARS microscopy for quantitative chemical imaging in human adipocytes," Biomed. Opt. Express **5**, 1378 (2014).
[25]T. Ideguchi, S. Holzner, B. Bernhardt, G. Guelachvili, N. Picqué, and T. W. Hänsch, "Coherent Raman spectro-imaging with laser frequency combs," Nature **502**, 355–358 (2013).
[26]M. J. Nasse, M. J. Walsh, E. C. Mattson, R. Reininger, A. Kajdacsy-Balla, V. Macias, R. Bhargava, and C. J. Hirschmugl, "High-resolution Fourier-transform infrared chemical imaging with multiple synchrotron beams," Nat. Methods **8**, 413–416 (2011).
[27]F. Ullah Khan, G. Guarnizo, and P. Martín-Mateos, "Direct hyperspectral dual-comb gas imaging in the mid-infrared," Opt. Lett. **45**, 5335 (2020).
[28]J. Yin, M. Zhang, Y. Tan, Z. Guo, H. He, L. Lan, and J.-X. Cheng, "Video-rate mid-infrared photothermal imaging by single-pulse photothermal detection per pixel," Sci. Adv. **9**, eadg8814 (2023).
[29]G. Ishigane, K. Toda, M. Tamamitsu, H. Shimada, V. R. Badarla, and T. Ideguchi, "Label-free mid-infrared photothermal live-cell imaging beyond video rate," Light Sci. Appl. **12**, 174 (2023).
[30]Y. Zhao, S. Kusama, Y. Furutani, W.-H. Huang, C.-W. Luo, and T. Fuji, "High-speed scanless entire bandwidth mid-infrared chemical imaging," Nat. Commun. **14**, 3929 (2023).
[31]M. Tamamitsu, Y. Sakaki, T. Nakamura, G. K. Podagatlapalli, T. Ideguchi, and K. Goda, "Ultrafast broadband Fourier-transform CARS spectroscopy at 50,000 spectra/s enabled by a scanning Fourier-domain delay line," Vib. Spectrosc. **91**, 163–169 (2017).
[32]A. Goyal, T. Myers, C. A. Wang, M. Kelly, B. Tyrrell, B. Gokden, A. Sanchez, G. Turner, and F. Capasso, "Active hyperspectral imaging using a quantum cascade laser (QCL) array and digital-pixel focal plane array (DFPA) camera," Opt. Express **22**, 14392 (2014).
[33]R. Zimmerleiter, R. Nikzad-Langerodi, C. Ruckebusch, M. Godejohann, J. Kilgus, K. Duswald, and M. Brandstetter, "QCL-based mid-infrared hyperspectral imaging of multilayer polymer oxygen barrier-films," Polym. Test. **98**, 107190 (2021).
[34]S. Junaid, S. Chaitanya Kumar, M. Mathez, M. Hermes, N. Stone, N. Shepherd, M. Ebrahim-Zadeh, P. Tidemand-Lichtenberg, and C. Pedersen, "Video-rate, mid-infrared hyperspectral upconversion imaging," Optica **6**, 702 (2019).
[35]D. Knez, A. M. Hanninen, R. C. Prince, E. O. Potma, and D. A. Fishman, "Infrared chemical imaging through non-degenerate two-photon absorption in silicon-based cameras," Light Sci. Appl. **9**, 125 (2020).
[36]E. O. Potma, D. Knez, Y. Chen, Y. Davydova, A. Durkin, A. Fast, M. Balu, B. Norton-Baker, R. W. Martin, T. Baldacchini, and D. A. Fishman, "Rapid chemically selective 3D imaging in the mid-infrared," Optica **8**, 995–1002 (2021).
[37]A. S. Kowligy, D. R. Carlson, D. D. Hickstein, H. Timmers, A. J. Lind, P. G. Schunemann, S. B. Papp, and S. A. Diddams, "Mid-infrared frequency combs at 10 GHz," Opt. Lett. **45**, 3677 (2020).
[38]F. U. Khan, A. Moreno-Oyervides, O. E. Bonilla-Manrique, and P. Martín-Mateos, "Sub-GHz optical resolution mid-infrared hyperspectral imaging with dual-comb," Opt. Lasers Eng. **170**, 107799 (2023).
[39]D. R. Carlson, D. D. Hickstein, and S. B. Papp, "Broadband, electro-optic, dual-comb spectrometer for linear and nonlinear measurements," Opt. Express **28**, 29148 (2020).
[40]M. Yu, Y. Okawachi, A. G. Griffith, N. Picqué, M. Lipson, and A. L. Gaeta, "Silicon-chip-based mid-infrared dual-comb spectroscopy," Nat. Commun. **9**, 1869 (2018).
[41]M. Yu, Y. Okawachi, A. G. Griffith, M. Lipson, and A. L. Gaeta, "Microfluidic mid-infrared spectroscopy via microresonator-based dual-comb source," Opt. Lett. **44**, 4259 (2019).
[42]N. R. Newbury, I. Coddington, and W. Swann, "Sensitivity of coherent dual-comb spectroscopy," Opt. Express **18**, 7929 (2010).
[43]A. J. Lind, A. Kowligy, H. Timmers, F. C. Cruz, N. Nader, M. C. Silfies, T. K. Allison, and S. A. Diddams, "Mid-infrared frequency comb generation and spectroscopy with few-cycle pulses and $\chi^{(2)}$ nonlinear optics," Phys. Rev. Lett. **124**, 133904 (2020).
[44]H. Timmers, A. Kowligy, A. Lind, F. C. Cruz, N. Nader, M. Silfies, G. Ycas, T. K. Allison, P. G. Schunemann, S. B. Papp, and S. A. Diddams, "Molecular fingerprinting with bright, broadband infrared frequency combs," Optica **5**, 727 (2018).
[45]N. Hoghooghi, P. Chang, S. Egbert, M. Burch, R. Shaik, S. A. Diddams, P. Lynch, and G. B. Rieker, "GHz repetition rate mid-infrared frequency comb spectroscopy of fast chemical reactions," Optica **11**, 876 (2024).
[46]D. M. B. Lesko, H. Timmers, S. Xing, A. Kowligy, A. J. Lind, and S. A. Diddams, "A six-octave optical frequency comb from a scalable few-cycle erbium fibre laser," Nat. Photonics **15**, 281–286 (2021).
[47]S. Xing, D. M. B. Lesko, T. Umeki, A. J. Lind, N. Hoghooghi, T.-H. Wu, and S. A. Diddams, "Single-cycle all-fiber frequency comb," APL Photonics **6**, 086110 (2021).

[48]N. B. Hébert, J. Genest, J.-D. Deschênes, H. Bergeron, G. Y. Chen, C. Khurmi, and D. G. Lancaster, "Self-corrected chip-based dual-comb spectrometer," Opt. Express **25**, 8168 (2017).
[49]N. B. Hébert, V. Michaud-Belleau, J.-D. Deschênes, and J. Genest, "Self-correction limits in dual-comb interferometry," IEEE J. Quantum Electron. **55**, 1–11 (2019).
[50]M. A. De Araújo, R. Silva, E. De Lima, D. P. Pereira, and P. C. De Oliveira, "Measurement of Gaussian laser beam radius using the knife-edge technique: Improvement on data analysis," Appl. Opt. **48**, 393 (2009).
[51]A. Tourigny-Plante, P. Guay, and J. Genest, "Apodization in dual-comb spectroscopy for rapid measurement," in *Optical Sensors and Sensing Congress* (Optica Publishing Group, Washington, DC, 2020), paper LTu3C.2.
[52]E. D. Caldwell, L. C. Sinclair, N. R. Newbury, and J.-D. Deschenes, "The time-programmable frequency comb and its use in quantum-limited ranging," Nature **610**, 667 (2022).
[53]F. R. Giorgetta, J.-D. Deschênes, R. L. Lieber, I. Coddington, N. R. Newbury, and E. Baumann, "Broadband dual-comb hyperspectral imaging and adaptable spectroscopy with programmable frequency combs," APL Photonics **9**, 010805 (2024).